

# Constraint on the early-formed dark matter halos using the free-free emission in the Planck foreground analysis

Katsuya T. Abe,<sup>\*</sup> Teppei Minoda<sup>✉</sup>, and Hiroyuki Tashiro

*Division of Particle and Astrophysical Science, Graduate School of Science, Nagoya University, Chikusa, Nagoya 464-8602, Japan*

 (Received 10 August 2021; accepted 3 March 2022; published 28 March 2022)

We provide a new constraint on the small-scale density fluctuations, evaluating the diffuse background free-free emission from dark matter halos in the dark ages. If there exists a large amplitude of the matter density fluctuations on small scales, the excess enhances the early formation of dark matter halos. When the virial temperature is sufficiently high, the gas in a halo is heated up and ionized by thermal collision. The heated ionized gas emits photons by the free-free process. We would observe the sum of these photons as the diffuse background free-free emission. Assuming the analytical dark matter halo model including the gas density and temperature profile, we calculate the intensity of the diffuse background free-free emission from early-formed dark matter halos in the microwave frequency range. Comparing with the recent foreground analysis on cosmic microwave background, we obtain the constraint on the excess of the density fluctuations on small scales. Our constraint corresponds to  $P_\zeta \lesssim 10^{-7}$  for  $k \simeq 1\text{--}100 \text{ Mpc}^{-1}$  with assuming the delta-function-type curvature power spectrum. Therefore, our constraint is the most stringent constraint on the perturbations below 1 Mpc scales.

DOI: [10.1103/PhysRevD.105.063531](https://doi.org/10.1103/PhysRevD.105.063531)

## I. INTRODUCTION

The primordial perturbations are the initial seeds of various cosmological structures: the temperature anisotropies of the cosmic microwave background (CMB), the large-scale structure (LSS), clusters of galaxies, galaxies, and so on. Therefore, the statistical properties of the primordial perturbations are well studied. In particular, the power spectrum of the primordial perturbations is one of the important statistics to understand the cosmological structure formation. It is thoroughly measured on LSS through the observations of the CMB on  $10^{-3} \text{ Mpc}^{-1} \lesssim k \lesssim 10^{-1} \text{ Mpc}^{-1}$  [1] and the LSS (e.g., galaxy clustering, weak lensing, Ly- $\alpha$  forest and so on) on  $k \sim 1 \text{ Mpc}^{-1}$  [2–7].

These observations have revealed that the amplitude of the power spectrum is in order of  $P_\zeta \sim 10^{-9}$  on those scales and is almost scale-invariant. These statistical natures are consistent with the primordial perturbations predicted in the inflationary paradigm [8,9]. On the other hand, on smaller scales with  $k > 1 \text{ Mpc}^{-1}$ , the primordial perturbations are not known well. Many studies suggest that the excess power on small scales can be induced by a lot of mechanisms in the early universe: multifield inflation [10], phase transition [11,12], early matter-dominated era [13], fast-rolling scalar field domination [14], and so on. Therefore, the investigation of the primordial perturbations

on small scales can improve our knowledge of the primordial universe.

One of the powerful probes for the small-scale perturbations is the CMB distortion [15–17]. The small-scale primordial perturbations are damped out by the Silk damping, however, instead, the distortion of the CMB energy spectrum would be created. Therefore, measurements of the CMB distortion lead us to further understanding of the primordial perturbations [18–22]. For example, Ref. [19] has pointed out that the CMB distortion measurement by COBE/FIRAS [23,24] provides the constraint in order of  $P_\zeta \lesssim 10^{-5}$  for the wave number range,  $k \approx 1\text{--}10^4 \text{ Mpc}^{-1}$ , and next-generation CMB measurements like PIXIE [25] can be a probe of the level of the scale-invariant spectrum,  $P_\zeta \lesssim 10^{-8}$ . Another hopeful measurement is future redshifted 21-cm observations which are expected to explore the density perturbations on smaller scales than the Silk scale [26]. Since the 21-cm signal comes from neutral hydrogen, the measurements of the spatial fluctuations in the redshifted 21-cm signal can trace the density fluctuations before the epoch of reionization. In order to measure the fluctuations of 21-cm signals from high redshifts, the radio interferometer telescope, the Square Kilometre Array (SKA), is now under construction.

The large amplitude of the perturbations on small scales promotes the structure formation and produces substantial collapsed objects in the early universe. One of such collapsed objects is a primordial black hole (PBH) [27]. PBHs are considered to be responsible for a non-negligible

<sup>\*</sup>abe\_kt@nagoya-u.jp

fraction of dark matter (DM) compositions [28,29]. Furthermore, they are attracting attention, because of the recent detection of gravitational wave (GW) events via LIGO and Virgo collaboration [30], as sources of GWs. The abundance of PBHs has been studied in a wide range of the PBH mass scale [31]. Since the PBH mass scale corresponds to the scale of the overdense region collapsing to PBHs, the constraint on the PBH abundance can be converted to the limit on the perturbations in the wide range of the scale [32]. However, the PBH formation requires large amplitude of curvature power spectrum as  $P_\zeta \sim 10^{-2} - 10^{-1}$ . Therefore, their constraint on the perturbations is relatively not so tight.

The density fluctuations are induced by the primordial perturbations and grow gravitationally well after the matter-radiation equality. In the growth, the overdense region on small scales finally collapses into the nonlinear structures called ultra-compact minihalos or minihalos in higher redshifts than the standard hierarchical structure formation due to the scale-invariant primordial perturbations [33]. With the self-annihilating DM model, the abundance of these early-formed DM halos is constrained by the present gamma-ray observations. Accordingly, the limit on the primordial perturbations can be obtained with the formation scenario [34–36]. However, the constraint on the primordial perturbations highly depends on the parameters of the self-annihilating DM. The constraint on the early-formed DM halo abundance, which is independent of the DM model can be obtained from redshifted 21-cm observations. Depending on their mass, early-formed DM halos can host abundant neutral hydrogen gas. Therefore, redshifted 21-cm observations can probe the abundance of early-formed DM halos [37]. Several studies have shown that SKA can provide the stringent limit on the abundance of early-formed collapsed objects and the amplitude of the primordial perturbations [38–41].

In this paper, we discuss the diffuse background free-free emission in the CMB frequency range from early-formed DM halos. In the formation of DM halos, baryonic gas is collapsed into them. During the collapse, the gas is heated up by the gravitational potential and ionized by the collisions between gas particles if the halo virial temperature is high enough, as  $T_{\text{vir}} \gtrsim 10^4$  K. Such hot ionized gas can emit photons via free-free emission, and they would be observed as the diffuse background free-free emission.

The diffuse background free-free emission has already been identified as one of the important foreground components in the CMB analysis [42,43]. Although most of the observed free-free emission is believed to be Galactic origin, a lot of cosmological free-free emitters can be considered, for example, the intergalactic medium (IGM) [44], the galaxy groups and clusters after the reionization [45], and the structure formation during the reionization [46]. The estimated amplitude is roughly 10% level of the observed free-free emission component.

Here, we focus on the early-formed DM halos with  $M_{\text{halo}} \sim 10^7 - 10^{13} M_\odot$  and estimate the contribution to the observed free-free emission component in the CMB frequency range. These mass scales roughly correspond to the perturbation scales  $k \sim 1 - 100 \text{ Mpc}^{-1}$  and there is a possible window for the excess of the primordial perturbations to produce DM halos much earlier than in the standard hierarchical structure formation scenario. Comparing our estimation of the diffuse background free-free emission with the observed free-free emission component [42,43], we obtain the constraint on the primordial density fluctuations on small scales.

The rest of this paper is organized as follows. In Sec. II, we provide the halo model describing the density, temperature, and ionization fraction of gas by assuming the hydrostatic equilibrium, and the collisional-ionization equilibrium with isothermal gas. Then, we calculate the intensity of the free-free emission from individual halos for different mass  $M_{\text{halo}}$  and formation redshift  $z_f$ . Next, in Sec. III, considering the halo formation history, we formulate the diffuse background intensity which is the sum of the free-free emission from early-formed halos. The results are shown in Sec. IV. We also discuss the application of our results to the constraint on the primordial curvature perturbations and obtain the limit by comparing the intensity of the observed free-free emission in the CMB frequency range. We conclude in Sec. V. Throughout this paper, we take the flat  $\Lambda$ CDM model with:  $(\Omega_m, \Omega_b, h, n_s, \sigma_8) = (0.32, 0.049, 0.67, 0.97, 0.81)$  [47].

## II. FREE-FREE EMISSION FROM THE INDIVIDUAL HALO

In this section, we estimate the intensity of the free-free emission from individual halos. It depends on the number density and temperature profiles of ionized gas. First, we construct the simple analytical model of ionized gas in a DM halo with mass  $M_{\text{halo}}$ .

### A. Gas structure of DM halo

Suppose that a DM halo forms with a mass of  $M_{\text{halo}}$  in a redshift  $z_f$ . We assume that, after the virialization, the DM density profile is given by the NFW profile [48],

$$\rho_{\text{NFW}}(r) = \frac{\rho_s}{\frac{r}{r_s} (1 + \frac{r}{r_s})^2}, \quad (1)$$

where  $r_s$  is the scale radius, which is related to the virial radius

$$R_{\text{vir}}(M_{\text{halo}}) = \left( \frac{3M_{\text{halo}}}{4\pi\Delta_c\rho_m(z_f)} \right)^{1/3}, \quad (2)$$

with the matter density  $\rho_m(z)$  and the concentration parameter,  $c_s \equiv R_{\text{vir}}/r_s$ .

The scale density  $\rho_s$  is given by

$$\rho_s = \frac{M_{\text{halo}}}{4\pi r_s^3 F(c_s)} = \frac{c_s^3}{3F(c_s)} \Delta_c \rho_m(z_f), \quad (3)$$

where  $\Delta_c = 18\pi^2$  is the spherical overdensity of the halo, and the function  $F(x)$  is described as

$$F(x) = \ln(1+x) - \frac{x}{1+x}. \quad (4)$$

The concentration parameter  $c_s$  varies depending on the mass and redshift of the halo. Although no simulation covers both the mass and redshift range we are interested in this paper, Ref. [49] has performed N-body simulations and suggested the mass-concentration relation from the simulation results including DM halos with mass  $M_{\text{halo}} > 10^9 M_\odot$  in the redshift range of  $0 < z < 14$ . This relation is based on the analytic form given in Ref. [50], and in this model, the concentration parameter depends on the spectral index of the primordial curvature power spectrum. Because this concentration parameter becomes larger as the spectral index increases, we conservatively take the concentration parameter for the scale-invariant case to reduce the impact of the concentration parameter on our final results.

In the halo formation, the gas in a DM halo is heated to the virial temperature by the virial shock. The virial temperature  $T_{\text{vir}}$  is given by [51]

$$T_{\text{vir}}(M_{\text{halo}}, z_f) = 1.98 \times 10^4 \left( \frac{\mu}{0.6} \right) \left( \frac{M_{\text{halo}}}{10^8 h^{-1} M_\odot} \right)^{2/3} \times \left[ \frac{\Omega_m}{\Omega_m(z_f)} \frac{\Delta_c}{18\pi^2} \right]^{1/3} \left( \frac{1+z_f}{10} \right) \text{K}, \quad (5)$$

where  $\mu$  is the mean molecular weight (we set  $\mu = 0.6$ ),  $\Omega_m(z)$  is the matter density parameter at a redshift  $z$  after the matter-dominant era,

$$\Omega_m(z) = \frac{\Omega_m(1+z)^3}{\Omega_m(1+z)^3 + \Omega_\Lambda}, \quad (6)$$

with  $\Omega_m = \Omega_m(z=0)$ ,  $k_B$  is the Boltzmann constant, and  $m_p$  is mass of proton.

To determine the gas density profile in a DM halo, we make the assumption that the gas in the DM halo has an isothermal profile with the virial temperature  $T_{\text{vir}}$  and is in the hydrostatic equilibrium between the gas pressure and the DM potential of the NFW profile. Under these conditions, the gas number density profile is given in the analytical form [52],

$$n_{\text{gas}}(r) = n_{\text{gas},0} \exp \left[ -\frac{\mu m_p}{2k_B T_{\text{vir}}} (V_{\text{esc}}^2(0) - V_{\text{esc}}^2(r)) \right]. \quad (7)$$

Here,  $V_{\text{esc}}$  is the escape velocity written by

$$V_{\text{esc}}^2(r) = 2 \int_r^\infty \frac{GM(r')}{r'^2} dr' = \frac{2GM_{\text{halo}} F(c_s x_r) + c_s x_r / (1 + c_s x_r)}{R_{\text{vir}} x_r F(c_s)}, \quad (8)$$

where  $x_r = r/R_{\text{vir}}$ , and  $M(r) = \int_0^r 4\pi r'^2 \rho_{\text{gas}}(r') dr'$ .

The number density at the central core,  $n_{\text{gas},0}$ , in Eq. (7) is obtained by fixing the total gas mass in the sphere with  $R_{\text{vir}}$  to  $M_{\text{gas}} = M_{\text{halo}} \Omega_b / \Omega_m$ ,

$$n_{\text{gas},0}(z) = \frac{(\Delta_c/3) c_s^3 e^A}{\int_0^{c_s} (1+t)^A / t^2 dt} \left( \frac{\Omega_b}{\Omega_m} \right) \frac{\rho_{\text{cri}}(z)}{m_p}, \quad (9)$$

where  $A \equiv V_{\text{esc}}^2(0) R_{\text{vir}} / GM_{\text{halo}} = 2c_s / F(c_s)$ .

In this work, we assume that DM halos do not host any stars in themselves for simplicity. In the absence of ionization photon sources including stars, collisional ionization is a possible process to ionize the gas in a DM halo. Since the collisional ionization and recombination time-scales are sufficiently shorter than the cosmological time-scale, we may assume that halo gas is in the steady-state, by balancing between the collisional ionization and the case-B recombination. In such a case, the ionization fraction in a DM halo with the temperature  $T_{\text{halo}}$  is determined by

$$x_e(T_{\text{halo}}) = \frac{\tilde{C}_{\text{coll}}}{\tilde{C}_{\text{coll}} + \tilde{A}_{\text{rec}}}, \quad (10)$$

where  $\tilde{C}_{\text{coll}} = C_{\text{coll}} / (1 - x_e)$ , and  $C_{\text{coll}}$  is the electron-collisional ionization rate which is given by the fitting formula [53],

$$C_{\text{coll}} \approx 5.85 \times 10^{-9} T_4^{1/2} e^{-T_H/T_{\text{halo}}} n_{\text{gas}} (1 - x_e) \text{ cm}^3/\text{s}. \quad (11)$$

Here,  $T_H \approx 1.58 \times 10^5 \text{ K}$  and  $T_4 \equiv T_{\text{halo}}/10^4 \text{ K}$ . In Eq. (11),  $\tilde{A}_{\text{rec}} = A_{\text{rec}}/x_e$ , and  $A_{\text{rec}}$  is the recombination rate obtained by

$$A_{\text{rec}} = -\alpha_H n_{\text{gas}} x_e, \quad (12)$$

where  $\alpha_H$  is the case-B recombination coefficient for hydrogen and fitted by Ref. [54] as

$$\alpha_H = 1.14 \times 10^{-13} \frac{a T_4^b}{1 + c T_4^d} \text{ cm}^3/\text{s} \quad (13)$$

with the fitting parameters,  $a = 4.309$ ,  $b = -0.6166$ ,  $c = 0.6703$ , and  $d = 0.5300$ . In our model, the ionization fraction is only controlled by the gas temperature. When the gas temperature is larger than  $10^4 \text{ K}$ , the ionization fraction goes up close to the unity.

Although the gas becomes hot by the virial shock at the formation of the DM halo, the gas will be cooled down by the cooling mechanism related to baryon physics.

Assuming the cooling timescale  $t_{\text{cool}}$ , the temperature is expressed at a given redshift  $z$ ,

$$T_{\text{halo}}(M_{\text{halo}}, z, z_f) = T_{\text{vir}}(M_{\text{halo}}, z_f) \exp\left(-\frac{\Delta_t(z, z_f)}{t_{\text{cool}}}\right), \quad (14)$$

where  $\Delta_t$  is the cosmic time duration in the redshift range  $[z, z_f]$  in the matter dominated epoch,

$$\Delta_t \approx \frac{2}{3} \left( \frac{1}{H(z)} - \frac{1}{H(z_f)} \right), \quad (15)$$

with the Hubble parameter  $H(z)$ .

The main cooling mechanism depends on the redshift and the gas properties including the gas density, temperature, and ionization fraction. One of the main cooling mechanisms is the free-free emission cooling. The timescale might be defined by

$$t_{\text{ff}}(M, z) = \frac{3/2 n_{\text{gas}} T_{\text{halo}}}{\int d\nu \epsilon_{\nu}^{\text{ff}}}, \quad (16)$$

where  $\epsilon_{\nu}^{\text{ff}}$  is the efficiency of free-free emission which is defined in the following subsection, especially in Eq. (18). When the gas is ionized (even if partially), the Compton cooling by CMB photons also can be the main cooling mechanism. In this case, the cooling timescale depends on only the redshift,

$$t_{\text{Comp}}(z) = \frac{3m_e c}{4\sigma_T \rho_{\gamma}} f_{\text{cool}} \simeq 1.4 \times 10^7 f_{\text{cool}} \left( \frac{1+z}{20} \right)^{-4} \text{yr}, \quad (17)$$

where  $m_e$  is the mass of electron,  $\rho_{\gamma}$  is the CMB energy density, and  $f_{\text{cool}} \equiv (1+x_e)/2x_e$  represents the dependence on the ionized fraction. Here we assume that the baryon is composed of only hydrogen atoms.

Through the paper, we adopt the cooling timescale for the smaller value of Eqs. (16) and (17), that is,  $t_{\text{cool}} = \min(t_{\text{ff}}, t_{\text{Comp}})$ . Because of the cooling, even if the gas temperature is high enough to ionize the gas at the formation time, the temperature decreases, and finally the gas becomes neutral by following Eq. (10).

As we mentioned above, we assume that stars are not formed in DM halos, and we consider only the Compton cooling as the cooling process. However, when the virial temperature is larger than  $10^4$  K, the atomic cooling becomes effective and leads to further collapsing of the gas and the star formation. Stars could heat up and ionize the gas in such massive DM halos substantially. While that can lead to enhance the free-free emission, the timescale and the efficiency of the star formation are still uncertain. Therefore, we do not include these effects.

## B. Free-free emission

When the gas in DM halos has a high temperature enough for the collisional ionization, the ionized gas can emit radiation through thermal free-free emission. The emissivity of the thermal free-free emission at a frequency  $\nu$  is given by [55]

$$\epsilon_{\nu}^{\text{ff}} = \frac{2^3 e^6}{3m_e c^3} \left( \frac{2\pi}{3m_e k_B T_{\text{halo}}} \right)^{1/2} \times x_e^2 n_{\text{gas}}^2 \exp(-h_p \nu / k_B T_{\text{halo}}) \bar{g}_{\text{ff}}, \quad (18)$$

where  $h_p$  is the Planck constant. In this paper, we are interested in the CMB frequency range or below them. Since these frequencies are much smaller than the halo temperature for the free-free emission,  $h_p \nu \ll k_B T_{\text{halo}}$ , we take  $\exp(-h_p \nu / k_B T_{\text{halo}}) \approx 1$ . In Eq. (18),  $\bar{g}_{\text{ff}}$  is a velocity-averaged Gaunt factor. Reference [56] has provided the fitting formula for the  $\bar{g}_{\text{ff}}$ ,

$$\bar{g}_{\text{ff}} = \log\{\exp[5.960 - \sqrt{3}/\pi \log(\nu_9 T_4^{-3/2})] + e\}, \quad (19)$$

where  $\nu_9 \equiv \nu/(1 \text{ GHz})$ , and  $e$  is the Napier's constant. Since, in our gas model, the number density has radial dependence, the emissivity also depends on the radius in a DM halo.

Now we calculate the mean intensity of the free-free emission from a DM halo. When the optical depth of the free-free absorption is negligible, the mean intensity of the free-free emission induced by an individual halo is obtained by

$$I_{\nu}^{\text{ind}}(z, z_f, M_{\text{halo}}) = \frac{\int \epsilon_{\nu}^{\text{ff}} dV}{S_{\text{halo}}}, \quad (20)$$

where  $S_{\text{halo}}$  is the physical cross section of a DM halo on the sky,  $S_{\text{halo}} = \pi R_{\text{vir}}^2$ .

Since the gas profile depends on the redshift of the emission  $z$ , the formation redshift  $z_f$ , and the mass of the DM halos  $M_{\text{halo}}$ , Eq. (20) depends on these parameters.

## III. DIFFUSE BACKGROUND FREE-FREE EMISSION

Now we consider the diffuse background intensity emitted from DM halos with mass  $M_{\text{halo}}$  residing spherical shell between from  $z$  to  $z + dz$ . This intensity is obtained by integrating the contributions from the DM halos formed until redshift  $z$ ,

$$dI_{\nu}^{\text{ff}}(z, M_{\text{halo}}) = \left( \int_z^{\infty} f_{\text{sky}} I_{\nu}^{\text{ind}} \frac{dn_{\text{halo}}^{\text{com}}}{dz_f} dz_f \right) \frac{dV_{\text{com}}}{dz} dz. \quad (21)$$

Here, we omit the dependencies of  $f_{\text{sky}}$  and  $I_{\nu}^{\text{ind}}$  on  $(z, z_f, M_{\text{halo}})$ . In Eq. (21),  $V_{\text{com}}$  is the total comoving volume out to redshift  $z$ , and  $n_{\text{halo}}^{\text{com}}$  is the comoving number

density of halos with mass  $M_{\text{halo}}$  at a redshift  $z$ , which we discuss later. Additionally,  $f_{\text{sky}}$  in Eq. (21) is the sky fraction of the DM halos formed at  $z_f$  with mass  $M_{\text{halo}}$  and given by

$$f_{\text{sky}} = \frac{\Omega_{\text{halo}}}{4\pi}, \quad (22)$$

where the solid angle  $\Omega_{\text{halo}}(z, z_f, M_{\text{halo}})$  of a DM halo is given by  $\Omega_{\text{halo}} = \pi((1+z)R_{\text{vir}})^2/\chi^2$  with the comoving distance  $\chi$ , from  $z=0$  to  $z$ .

Taking into account the redshift effect due to the cosmological expansion, the diffuse background intensity at the observed frequency  $\nu_{\text{obs}}$  is calculated by

$$I_{\text{obs}}(\nu_{\text{obs}}) = \int_{z_{\text{cut}}}^{\infty} dz \frac{1}{(1+z)^3} \frac{dJ_{\nu_{\text{em}}}^{\text{ff}}(z, M_{\text{halo}})}{dz}, \quad (23)$$

where  $\nu_{\text{em}} = (1+z)\nu_{\text{obs}}$ , and  $z_{\text{cut}}$  is the lower limit of the redshift. We are interested in the free-free emission from DM halos created by the excess fluctuations from the scale-invariant spectrum. Therefore, we set  $z_{\text{cut}}$  to the redshift at which the mass variance due to the scale-invariant spectrum reaches the critical density contrast  $\delta_c = 1.69$ , so that  $\delta_c = \sigma_i(z, M_{\text{halo}})$ , where  $\sigma_i(z, M)$  is the mass variance calculated from the scale-invariant spectrum at  $z$ .

### A. DM halo number density

In order to calculate the number density of DM halos in Eq. (21), we assume that the density fluctuations obey Gaussian statistics. We represent the mass variance with mass  $M_{\text{halo}}$  at the present epoch as  $\sigma_0(M_{\text{halo}})$ . The mass variance at a redshift  $z$  is  $\sigma(z, M_{\text{halo}}) = D(z)\sigma_0(M_{\text{halo}})$  with the linear growth rate  $D(z)$  which is normalized as  $D(0) = 1$  at the present. Using the spherical collapse model, at a redshift  $z_f$  in the matter dominated epoch, the mass fraction of DM halos with mass  $> M_{\text{halo}}$  is given by

$$f_{\text{coll}}(z_f, M_{\text{halo}}) = \text{erfc}\left(\frac{\nu_c}{\sqrt{2}}\right), \quad (24)$$

where  $\nu_c \equiv \delta_c/\sigma(z, M_{\text{halo}})$ .

The mass distribution of DM halos depends on the shape of the mass variance as a function of  $M_{\text{halo}}$ . However in this work, instead of specifying the shape of the mass variance, we simply assume that the number density of DM halos with mass  $M_{\text{halo}}$  is given by

$$n_{\text{halo}}^{\text{com}}(z_f, M_{\text{halo}}) = \Omega_m \frac{\rho_{\text{crit}}}{M_{\text{halo}}} f_{\text{coll}}(z_f, M_{\text{halo}}). \quad (25)$$

Since the mass fraction,  $\sigma(M_{\text{halo}})$  includes the contribution from not only dark matter halos with  $M_{\text{halo}}$  but also with  $M > M_{\text{halo}}$ , this evaluation leads to overestimate the number density of  $M_{\text{halo}}$ . In other words, we neglect the DM halos with  $M > M_{\text{halo}}$  in the above treatment.

However, the free-free intensity is larger for massive halos than that for lighter mass. We discuss this point in the next section. Therefore, the obtained intensity is the lowest signals of the free-free emission for the given mass variance with a single mass  $M_{\text{halo}}$ . Consequently, the limit on the primordial curvature perturbations would be estimated conservatively.

Accordingly, the derivative of the number density with respect to the formation redshift,  $z_f$  is

$$\frac{dn_{\text{halo}}^{\text{com}}}{dz_f} = \sqrt{\frac{2}{\pi}} \frac{\Omega_m \rho_{\text{crit}}}{M_{\text{halo}}} \nu_{c,0} \exp\left(-\frac{\nu_c^2}{2}\right), \quad (26)$$

where  $\nu_{c,0} = \delta_c/\sigma_0(M_{\text{halo}})$ . Through this halo number density, the diffuse background intensity from early-formed DM halos depends on the density fluctuations, whose statistical property we represent by two parameters ( $M_{\text{halo}}, \sigma_0(M_{\text{halo}})$ ).

In the next section, we demonstrate that the observation of the all-sky averaged free-free emission is a powerful probe of the density fluctuations on small scales, calculating the amplitude of the diffuse background intensity with different sets of two parameters [ $M_{\text{halo}}, \sigma_0(M_{\text{halo}})$ ].

## IV. RESULTS AND DISCUSSION

In Fig. 1, we show the dependence of the diffuse background intensity from early-formed DM halos at

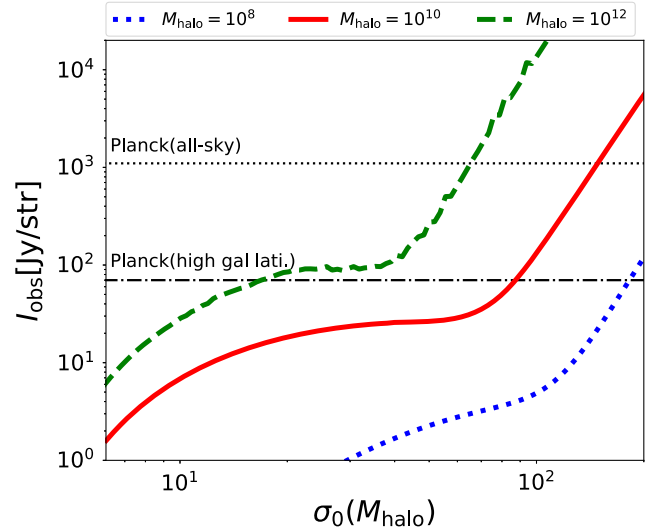


FIG. 1. The diffuse background intensity in Eq. (23) with different parameter sets ( $M_{\text{halo}}, \sigma_0(M_{\text{halo}})$ ) at  $\nu = 70$  GHz. The blue dotted line shows the intensity as a function of  $\sigma_0$  with  $M_{\text{halo}} = 10^8 M_{\odot}$ . The red solid and green dashed lines show the ones with  $M_{\text{halo}} = 10^{10}, 10^{12} M_{\odot}$  respectively. The thin black dotted line shows the intensity of the all-sky averaged free-free emission observed by the Planck satellite, and the thin black dash-dotted line shows the intensity averaged only in high galactic latitude region. See Fig. 4 for the detail.

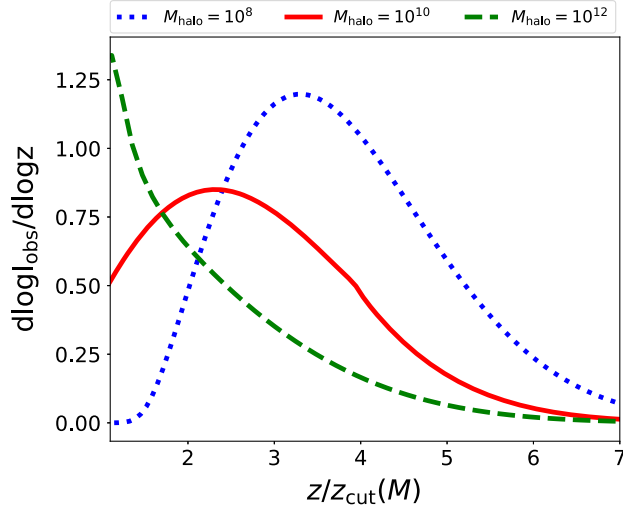


FIG. 2. The redshift distribution of the diffuse background intensity induced by early-formed halos with mass and mass variance  $(M_{\text{halo}}[M_{\odot}], \sigma_0) = (10^8, 24.8), (10^{10}, 19.5), (10^{12}, 14.2)$ . The color and line styles are the same as in Fig. 1.

$\nu = 70$  GHz on the mass variance  $\sigma_0(M)$  for different  $M = M_{\text{halo}}$ . It is worth mentioning that, in the standard  $\Lambda$ CDM model consistent with the Planck data, the mass variance are  $\sigma_0(M) = 12.0, 6.5$  and  $3.5$  for  $M = 10^{10}, 10^{11}$  and  $10^{12} M_{\odot}$ , respectively. When  $\sigma_0(M)$  becomes large, the formation of DM halos with mass  $M$  would start in higher redshifts, and the number density of DM halos emitting the free-free emission would increase. Therefore, the large  $\sigma_0(M)$  enhances the amplitude of the diffuse background intensity in these mass scales. Figure 1 tells us that more massive halos emit the stronger free-free intensity than less massive halos. This reason can be interpreted that the massive halos have higher virial temperature at their formation time, and they survive longer until the cooling down and the neutralization of the baryon gas.

Additionally, Fig. 2 shows the redshift distribution of the diffuse background intensity with at each redshift for  $M_{\text{halo}} = 10^8, 10^{10}$ , and  $10^{12} M_{\odot}$ . In this figure, we fix the mass variance as  $\sigma_0 = 24.8, 19.5$ , and  $14.2$ , respectively.

Figure 3 presents the frequency dependence of the diffuse background intensity in the CMB frequency range. These frequencies are smaller than  $k_B T_{\text{halo}}/h_p$ . Therefore, the frequency dependence comes from only the Gaunt factor of Eq. (19). The dependence is the same as in the free-free emission component in the CMB data analysis [42].

In the Planck CMB analysis, the free-free emission component has been separated from other diffuse foreground emissions. The obtained intensity map of the free-free emission tells us that the emission is strongly anisotropic. At low galactic latitude, the emission is strong, while the emission becomes weak as the galactic latitude increases. From the Planck data, the all-sky averaged free-free emission component is identified as  $I_{\nu} \approx 10^3$  Jy/str at the frequency  $\nu = 70$  GHz [42,43]. To avoid the

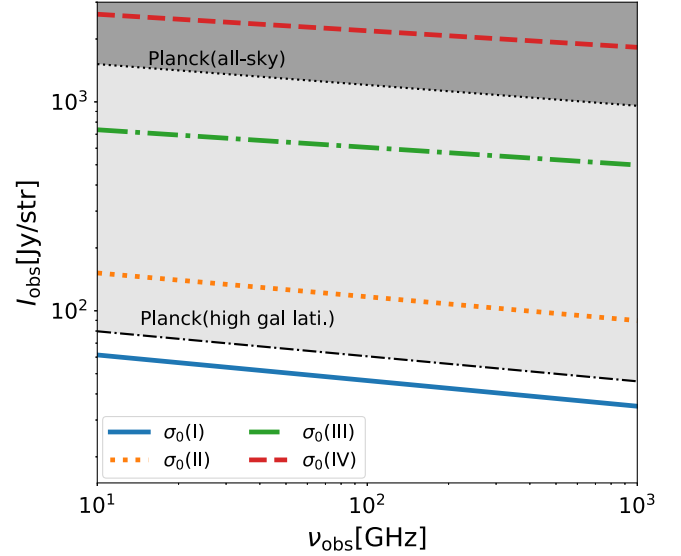


FIG. 3. The diffuse background intensity induced by early-formed halos with mass  $M_{\text{halo}} = 10^{12} M_{\odot}$ . The thick lines with different color and line types represent the diffuse background intensity with different amplitude of  $\sigma_0$ . From bottom to top, the lines are for  $\sigma_0(i) = (12.7, 41.7, 59.2, 73.0)$  with  $(i = \text{I, II, III, IV})$ . The thin black dotted line and the thin black dash-dotted line are the same as in Fig. 1.

contamination from the Galactic disk, we also calculate the intensity of the observed free-free emission component by masking the region at galactic latitude  $|b| < b_{\text{cut}}$ . Figure 4 shows the dependence of the averaged intensity on the cutoff galactic latitude  $b_{\text{cut}}$  at  $\nu = 70$  GHz. The averaged intensity becomes small as  $b_{\text{cut}}$  increases, and we have found that when we set  $b_{\text{cut}} > 60$  deg., so that the region with  $|b| < b_{\text{cut}}$  is masked, the resultant averaged intensity observed by Planck drops down roughly to 70 Jy/str (in the brightness temperature,  $T_b \sim 0.7 \times (\nu/70 \text{ GHz})^{-2} \mu\text{K}$ ). For comparison, we plot the intensity of the all-sky averaged free-free

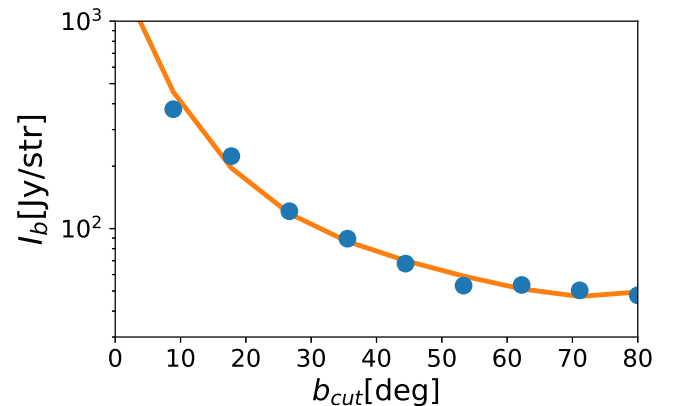


FIG. 4. The averaged intensity of the free-free emission from the Planck foreground map. The horizontal axis represents the absolute galactic latitude  $|b_{\text{cut}}|$  for masking the Galactic disk component. The orange line is the fitting curve for illustrative purposes.

emission  $I_\nu \approx 10^3$  Jy/str, and only in high galactic latitude,  $I_\nu \approx 70$  Jy/str as black dotted and dash-dotted lines, respectively, in Figs. 1 and 3.

Since the diffuse background intensity from early-formed DM halos cannot exceed the intensity of the observed free-free emission, we can obtain the constraint on  $\sigma_0(M_{\text{halo}})$ . Figure 5 represents the upper limit on the allowed  $\sigma_0(M_{\text{halo}})$  for each mass  $M_{\text{halo}}$ . The parameter sets in the colored region show the excluded ones where the diffuse background intensity is larger than the measured signal. It is noted that the dependence of the signal amplitude on the DM halo mass  $M_{\text{halo}}$  is weak in the mass range between  $10^{12} M_\odot$  and  $10^{13} M_\odot$ . This is because the free-free emission from individual halos gets higher as the halo mass increases, while the number density of DM halos decreases for a fixed  $\sigma_0$ . For halos with mass  $10^{11} M_\odot \lesssim M_{\text{halo}} \lesssim 10^{12} M_\odot$ , the diffuse background intensity weakly depends on the mass variance  $20 \lesssim \sigma_0 \lesssim 50$ , as shown in Fig. 1. Therefore the constraint on  $\sigma_0(M_{\text{halo}})$  strongly changes on these mass scales. Finally, in the lightest mass range as  $M_{\text{halo}} \lesssim 10^9 M_\odot$ , the virial temperature is not high enough to ionize the gas inside DM halos. Therefore, the signal strength decreases, and resultantly, the constraint on  $\sigma_0(M_{\text{halo}})$  quickly becomes weak.

We find that the fitting formula of the limitation of  $\sigma_0(M_{\text{halo}})$  by the intensity of the observed free-free emission averaged in all-sky is

$$\log_{10}\sigma_0 < -0.0061x^3 + 0.21x^2 - 2.56x + 12.43, \quad (27)$$

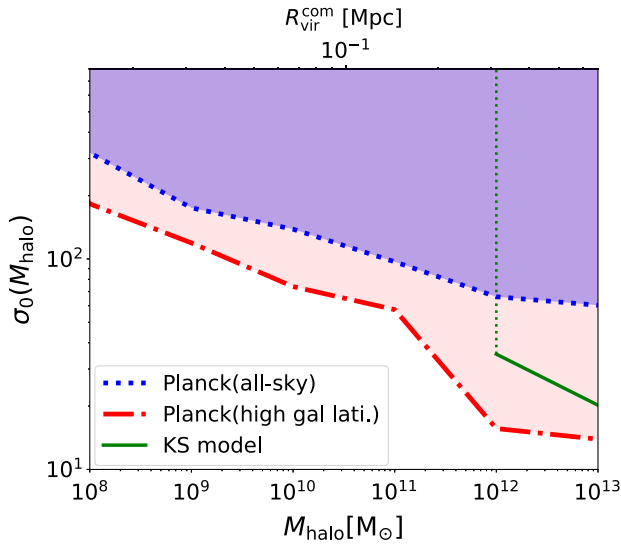


FIG. 5. The constraint on  $\sigma_0(M_{\text{halo}})$  from the observed free-free emission. The blue dotted line represents the limit from the Planck all-sky observation. The red dash-dotted line shows the one by the Planck observation only in the high galactic latitude region. The green solid line shows the same constraint as the red dash-dotted line but with the KS model for the gas profile in the DM halos. Below  $M_{\text{halo}} < 10^{12} M_\odot$ , the signals in the KS model are suppressed too strongly to obtain the constraint.

where  $x = \log_{10} M_{\text{halo}}$ . We mention that this fitting function can be adopted in the mass region  $M_{\text{halo}} = (10^8 M_\odot, 10^{13} M_\odot)$ .

We have obtained the constraint on the mass variance on  $M_{\text{halo}}$ . It is also worth discussing this constraint in terms of the primordial curvature perturbations. The mass variance is calculated from the power spectrum of the curvature perturbations  $\mathcal{P}_\zeta(k)$  by

$$\sigma_0^2(M) = \int d \log k \frac{4}{25} \frac{k^4}{\Omega_m^2 H_0^4} \mathcal{P}_\zeta(k) T^2(k) W_k^2(k R_M(M)), \quad (28)$$

where  $W_k(x)$  is the Fourier component of the top-hat window function, and  $R_M(M)$  is the comoving scale in which the mass  $M$  is enclosed with the background matter density  $\Omega_m \rho_{\text{cri}}$ . Besides, we adopt the transfer function for the matter density fluctuations  $T(k)$  as [57]

$$T(k) = \frac{45 \Omega_m^2 H_0^2}{2 \Omega_r k^2} \left( -\frac{7}{2} + \gamma_E + \ln \left( \frac{4\sqrt{\Omega_r} k}{\sqrt{3}\Omega_m H_0} \right) \right), \quad (29)$$

with the Euler-Mascheroni constant  $\gamma_E \simeq 0.577$ . Since we would like to constrain the excess of the fluctuations from the scale-invariant spectrum on small scales, we implicitly assume the blue-tilted power spectrum on these scales. In this case,  $\mathcal{P}_\zeta(k) W_k^2(kR)$  in Eq. (28) has a maximum value at  $k = 2\pi/R$ . Therefore, Eq. (28) can be approximated to

$$\sigma_0^2(M) \approx \frac{4}{25} \frac{k^4}{\Omega_m^2 H_0^4} \mathcal{P}_\zeta(k) T^2(k) \Big|_{k=k_p}, \quad (30)$$

where  $k_p = 2\pi/R_M(M_{\text{halo}})$  and we adopt the sharp- $k$  filter,  $k = k_p$ .

Using Eq. (30), we rewrite our constraint on  $\sigma_0(M_{\text{halo}})$  in Fig. 5 to the limit on the amplitude of the delta-function type primordial curvature power spectrum,  $\mathcal{P}_\zeta$  as a function of different  $k$ . Figure 6 is a summary of our constraint on the amplitude of the curvature perturbations. On scales  $1 \text{ Mpc}^{-1} < k < 100 \text{ Mpc}^{-1}$ , our constraint is stronger than the previous ones.

At the last of this section, we discuss the dependence of our results on the gas profile. The diffuse background intensity is proportional to the square of the number density of gas particle as shown in Eq. (18). We have evaluated the diffuse background intensity with the gas profile based on the hydrostatic equilibrium and the isothermal condition. In order to estimate the model uncertainty of the gas profile, we also calculate with the different gas profile model (KS model) suggested in Ref. [61]. In the KS model, without the isothermal condition, the gas density and temperature profiles are obtained from the hydrostatic equilibrium and the condition that the shape of the gas density profile becomes the same as the one of DM in the outer region of the DM halo. Calculating the diffuse background intensity

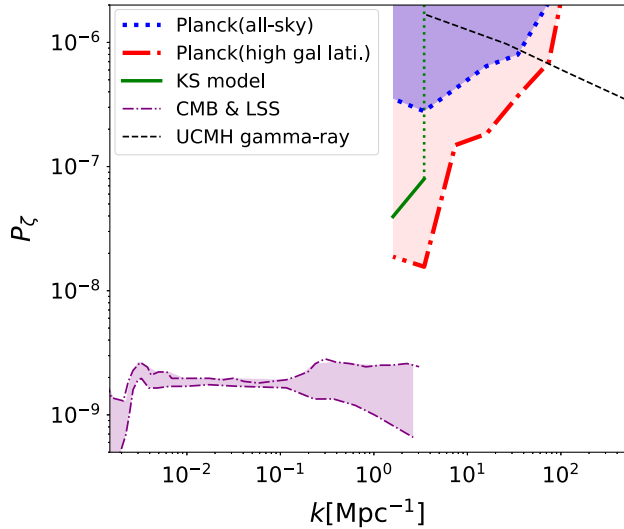


FIG. 6. The constraint on the primordial curvature power spectrum  $P_\zeta(k)$  through non-detection of the diffuse background intensity induced by early-formed DM halos with their mass of  $M_{\text{halo}}$ . The three thick lines: red dash-dotted, green solid, and blue dotted lines show the constraints by the same as in Fig. 5. The purple dash-dotted line and shaded region represent the allowed parameter region obtained from the CMB and LSS observation [58–60]. The black dashed line shows the one by the theoretical prediction of the gamma-ray induced by the UCMH with the self-annihilating DM model [36].

with this model and we find out that the signals become smaller than in the isothermal case. Although it depends on halo mass, the extent of the signal suppression is a factor of two in the mass range between  $10^{12} M_\odot < M < 10^{13} M_\odot$ . Comparing the free-free emission at the high galactic latitude, we obtain the constraint in the case of the KS model and plot it in Figs. 5 and 6. Because of the signal suppression, the constraint in the KS model is weaker than in the isothermal case as well.

## V. CONCLUSION

In this work, we have estimated the diffuse background free-free emission due to the early formation of DM halos. If there are a large amplitude of density fluctuations on small scales, DM halos form efficiently after the matter-radiation equality. Inside DM halos with high virial temperature, the gas is ionized by the thermal collision and can emit photons by the free-free process.

First, we construct the gas model in DM halos, assuming isothermal gas with the hydrostatic equilibrium and calculate the free-free emission from individual halos. In our model, the gas is heated up to the virial temperature at the halo formation and cooled down by the Compton scattering with CMB photons. The ionization of gas is achieved by thermal collisional ionization. The gas with a large virial temperature is ionized and can emit radiation through free-free emission. However since the Thomson scattering

cooled down the gas, the gas quickly becomes neutral and terminates the free-free emission. The intensity is completely determined by the halo mass and the formation redshift.

Next, assuming the excess of density fluctuations from the scale-invariant power spectrum on small scales, we have computed the diffuse background intensity.

Since it depends on the formation history of DM halos, the intensity is sensitive to the density fluctuations. We have found that the large mass variance promotes the DM halo formation at high redshifts, and increases the diffuse background intensity.

By comparing the intensity of the free-free emission observed by the Planck satellite, we have put an upper limit on the mass variance at the present epoch,  $\sigma_0(M)$ . The observed free-free emission is highly anisotropic and the intensity averaged only in high galactic latitude region is lower than that of the all-sky averaged free-free emission. We have shown that the comparison with the emission at high galactic latitude makes the constraint stronger. The obtained constraint on the mass variance from intensity averaged only in high galactic latitude region is  $\sigma_0 < 20$  in the mass range  $10^{12} M_\odot < M < 10^{13} M_\odot$ . This constraint allows us to provide the limit on the amplitude of the delta-function-type primordial curvature power spectrum,  $P_\zeta(k) \lesssim 10^{-7}$  for  $1 \text{ Mpc}^{-1} \lesssim k \lesssim 100 \text{ Mpc}^{-1}$ .

We have demonstrated that the measurements of the diffuse background free-free emission can probe the abundance of early-formed DM halos. However, there are several theoretical uncertainties related to the nonlinear structure formation in our estimation. One of such uncertainties is the baryon gas profile in DM halos. In order to investigate this uncertainty, we calculate the diffuse background intensity with a different gas profile model as in Ref. [61]. We have found that the difference of the gas profile models provides the suppression of the signal by a factor of two.

One way to improve the theoretical prediction of the diffuse background free-free emission is to perform numerical simulations of the early structure formation including baryon physics. Not only the gas profile mentioned above but also the star formation in early-formed DM halos can affect the diffuse background intensity because radiation from stars can heat up and ionize baryon gas inside halos. In addition, the further improvement of the constraint is expected by combining the other observational probes, 21-cm line observations, thermal and kinetic Sunyaev-Zel’dovich (SZ) effect, and so on. We leave them for our future work.

## ACKNOWLEDGMENTS

This work is supported by the Japan Society for the Promotion of Science (JSPS) KAKENHI Grants No. JP20J22260 (K. T. A), No. JP21K03533 (H. T), and No. JP21H05459 (H. T). This work is also supported by JSPS Overseas Research Fellowships (T.M).

- [1] N. Aghanim (Planck Collaboration), Planck 2018 results. VI. Cosmological parameters, *Astron. Astrophys.* **641**, A6 (2020).
- [2] P. McDonald, U. Seljak, S. Burles, D. J. Schlegel, D. H. Weinberg, R. Cen, D. Shih, J. Schaye, D. P. Schneider, N. A. Bahcall, J. W. Briggs, J. Brinkmann, R. J. Brunner, M. Fukugita, J. E. Gunn, Ž. Ivezić, S. Kent, R. H. Lupton, and D. E. Vanden Berk, The Ly $\alpha$  forest power spectrum from the Sloan Digital Sky Survey, *Astrophys. J. Suppl. Ser.* **163**, 80 (2006).
- [3] S. Chabanier, N. Palanque-Delabrouille, C. Yèche, J.-M. Le Goff, E. Armengaud, J. Bautista, M. Blomqvist, N. Busca, K. Dawson, T. Etourneau, A. Font-Ribera, Y. Lee, H. du Mas des Bourboux, M. Pieri, J. Rich, G. Rossi, D. Schneider, and A. Slosar, The one-dimensional power spectrum from the SDSS DR14 Ly $\alpha$  forests, *J. Cosmol. Astropart. Phys.* **07** (2019) 017.
- [4] B. Joachimi *et al.*, KiDS-1000 methodology: Modelling and inference for joint weak gravitational lensing and spectroscopic galaxy clustering analysis, *Astron. Astrophys.* **646**, A129 (2021).
- [5] M. Costanzi *et al.* (DES and SPT Collaborations), Cosmological constraints from DES Y1 cluster abundances and SPT multiwavelength data, *Phys. Rev. D* **103**, 043522 (2021).
- [6] M. Hilton *et al.*, The Atacama cosmology telescope: A catalog of > 4000 Sunyaev–Zel’dovich galaxy clusters, *Astrophys. J. Suppl. Ser.* **253**, 3 (2021).
- [7] T. M. C. Abbott *et al.* (DES Collaboration), Dark energy survey year 3 results: Cosmological constraints from galaxy clustering and weak lensing, *Phys. Rev. D* **105**, 023520 (2022).
- [8] A. A. Starobinsky, Dynamics of phase transition in the new inflationary universe scenario and generation of perturbations, *Phys. Lett.* **117B**, 175 (1982).
- [9] A. H. Guth and S. Y. Pi, Fluctuations in the New Inflationary Universe, *Phys. Rev. Lett.* **49**, 1110 (1982).
- [10] A. Ashoorioon, A. Krause, and K. Turzynski, Energy transfer in multi field inflation and cosmological perturbations, *J. Cosmol. Astropart. Phys.* **02** (2009) 014.
- [11] C. Schmid, D. J. Schwarz, and P. Widerin, Peaks above the Harrison-Zel’dovich Spectrum due to the Quark-Gluon to Hadron Transition, *Phys. Rev. Lett.* **78**, 791 (1997).
- [12] J. Barriga, E. Gaztañaga, M. G. Santos, and S. Sarkar, On the APM power spectrum and the CMB anisotropy: Evidence for a phase transition during inflation?, *Mon. Not. R. Astron. Soc.* **324**, 977 (2001).
- [13] G. Barenboim and J. Rasero, Structure formation during an early period of matter domination, *J. High Energy Phys.* **04** (2014) 138.
- [14] K. Redmond, A. Trezza, and A. L. Erickcek, Growth of dark matter perturbations during kination, *Phys. Rev. D* **98**, 063504 (2018).
- [15] J. Chluba and R. A. Sunyaev, The evolution of CMB spectral distortions in the early Universe, *Mon. Not. R. Astron. Soc.* **419**, 1294 (2012).
- [16] H. Tashiro, CMB spectral distortions and energy release in the early universe, *Prog. Theor. Exp. Phys.* **2014**, 6B107 (2014).
- [17] J. Chluba and D. Jeong, Teasing bits of information out of the CMB energy spectrum, *Mon. Not. R. Astron. Soc.* **438**, 2065 (2014).
- [18] W. Hu, D. Scott, and J. Silk, Power spectrum constraints from spectral distortions in the cosmic microwave background, *Astrophys. J.* **430**, L5 (1994).
- [19] J. Chluba, A. L. Erickcek, and I. Ben-Dayan, Probing the inflaton: Small-scale power spectrum constraints from measurements of the cosmic microwave background energy spectrum, *Astrophys. J.* **758**, 76 (2012).
- [20] E. Pajer and M. Zaldarriaga, New Window on Primordial Non-Gaussianity, *Phys. Rev. Lett.* **109**, 021302 (2012).
- [21] J. B. Dent, D. A. Easson, and H. Tashiro, Cosmological constraints from CMB distortion, *Phys. Rev. D* **86**, 023514 (2012).
- [22] J. Chluba and D. Grin, CMB spectral distortions from small-scale isocurvature fluctuations, *Mon. Not. R. Astron. Soc.* **434**, 1619 (2013).
- [23] D. J. Fixsen, E. S. Cheng, J. M. Gales, J. C. Mather, R. A. Shafer, and E. L. Wright, The cosmic microwave background spectrum from the full COBE FIRAS data set, *Astrophys. J.* **473**, 576 (1996).
- [24] J. C. Mather *et al.*, Measurement of the cosmic microwave background spectrum by the COBE FIRAS instrument, *Astrophys. J.* **420**, 439 (1994).
- [25] J. Chluba *et al.*, New horizons in cosmology with spectral distortions of the cosmic microwave background, *Exp. Astron.* **51**, 1515 (2021).
- [26] A. Loeb and M. Zaldarriaga, Measuring the Small-Scale Power Spectrum of Cosmic Density Fluctuations through 21 cm Tomography Prior to the Epoch of Structure Formation, *Phys. Rev. Lett.* **92**, 211301 (2004).
- [27] Y. B. Zel’dovich and I. D. Novikov, The hypothesis of cores retarded during expansion and the hot cosmological model, *Sov. Astron.* **10**, 602 (1967).
- [28] S. Hawking, Gravitationally collapsed objects of very low mass, *Mon. Not. R. Astron. Soc.* **152**, 75 (1971).
- [29] G. F. Chapline, Cosmological effects of primordial black holes, *Nature (London)* **253**, 251 (1975).
- [30] B. P. Abbott (LIGO Scientific, Virgo Collaborations), Observation of Gravitational Waves from a Binary Black Hole Merger, *Phys. Rev. Lett.* **116**, 061102 (2016).
- [31] B. Carr, K. Kohri, Y. Sendouda, and J. Yokoyama, Constraints on primordial black holes, *Rep. Prog. Phys.* **84**, 116902 (2021).
- [32] R. Emami and G. F. Smoot, Observational constraints on the primordial curvature power spectrum, *J. Cosmol. Astropart. Phys.* **01** (2018) 007.
- [33] M. Ricotti and A. Gould, A new probe of dark matter and high-energy universe using microlensing, *Astrophys. J.* **707**, 979 (2009).
- [34] P. Scott and S. Sivertsson,  $\gamma$  Rays from Ultracompact Primordial Dark Matter Minihalos, *Phys. Rev. Lett.* **103**, 211301 (2009).
- [35] A. S. Josan and A. M. Green,  $\gamma$  rays from ultracompact minihalos: Potential constraints on the primordial curvature perturbation, *Phys. Rev. D* **82**, 083527 (2010).
- [36] T. Bringmann, P. Scott, and Y. Akrami, Improved constraints on the primordial power spectrum at small scales

- from ultracompact minihalos, *Phys. Rev. D* **85**, 125027 (2012).
- [37] I. T. Iliev, P. R. Shapiro, A. Ferrara, and H. Martel, On the direct detectability of the cosmic dark ages: 21 centimeter emission from minihalos, *Astrophys. J.* **572**, L123 (2002).
- [38] T. Sekiguchi, H. Tashiro, J. Silk, and N. Sugiyama, Cosmological signatures of tilted isocurvature perturbations: Reionization and 21 cm fluctuations, *J. Cosmol. Astropart. Phys.* **03** (2014) 001.
- [39] H. Shimabukuro, K. Ichiki, S. Inoue, and S. Yokoyama, Probing small-scale cosmological fluctuations with the 21 cm forest: Effects of neutrino mass, running spectral index, and warm dark matter, *Phys. Rev. D* **90**, 083003 (2014).
- [40] T. Sekiguchi, T. Takahashi, H. Tashiro, and S. Yokoyama, 21 cm angular power spectrum from minihalos as a probe of primordial spectral runnings, *J. Cosmol. Astropart. Phys.* **02** (2018) 053.
- [41] K. Furugori, K. T. Abe, T. Tanaka, D. Hashimoto, H. Tashiro, and K. Hasegawa, The 21-cm signals from ultracompact minihaloes as a probe of primordial small-scale fluctuations, *Mon. Not. R. Astron. Soc.* **494**, 4334 (2020).
- [42] R. Adam *et al.* (Planck Collaboration), Planck 2015 results. X. Diffuse component separation: Foreground maps, *Astron. Astrophys.* **594**, A10 (2016).
- [43] Y. Akrami *et al.* (Planck Collaboration), Planck 2018 results. IV. Diffuse component separation, *Astron. Astrophys.* **641**, A4 (2020).
- [44] A. Cooray and S. R. Furlanetto, Free-free emission at low radio frequencies, *Astrophys. J.* **606**, L5 (2004).
- [45] P. P. Ponente, J. M. Diego, R. K. Sheth, C. Burigana, S. R. Knollmann, and Y. Ascasibar, The cosmological free-free signal from galaxy groups and clusters, *Mon. Not. R. Astron. Soc.* **410**, 2353 (2011).
- [46] B. Liu, J. Jaacks, S. L. Finkelstein, and V. Bromm, Global radiation signature from early structure formation, *Mon. Not. R. Astron. Soc.* **486**, 3617 (2019).
- [47] N. e. a. Aghanim (Planck Collaboration), Planck 2018 results. VI. Cosmological parameters, *Astron. Astrophys.* **641**, A6 (2020).
- [48] J. F. Navarro, C. S. Frenk, and S. D. M. White, A universal density profile from hierarchical clustering, *Astrophys. J.* **490**, 493 (1997).
- [49] T. Ishiyama, F. Prada, A. A. Klypin, M. Sinha, R. B. Metcalf, E. Jullo, B. Altieri, S. A. Cora, D. Croton, S. de la Torre, D. E. Millán-Calero, T. Oogi, J. Ruedas, and C. A. Vega-Martínez, The Uchuu simulations: Data release 1 and dark matter halo concentrations, *Mon. Not. R. Astron. Soc.* **506**, 4210 (2021).
- [50] B. Diemer and M. Joyce, An accurate physical model for halo concentrations, *Astrophys. J.* **871**, 168 (2019).
- [51] J. L. Johnson, Formation of the first galaxies: Theory and simulations, in *The First Galaxies*, Astrophysics and Space Science Library Vol. 396, edited by T. Wiklind, B. Mobasher, and V. Bromm (Springer, Berlin, Heidelberg, 2013), p. 177, [10.1007/978-3-642-32362-1](https://doi.org/10.1007/978-3-642-32362-1).
- [52] N. Makino, S. Sasaki, and Y. Suto, X-ray gas density profile of clusters of Galaxies from the Universal Dark Matter Halo, *Astrophys. J.* **497**, 555 (1998).
- [53] K. L. Bell, H. B. Gilbody, J. G. Hughes, A. E. Kingston, and F. J. Smith, Recommended data on the electron impact ionization of light atoms and ions, *J. Phys. Chem. Ref. Data* **12**, 891 (1983).
- [54] D. Pequignot, P. Petitjean, and C. Boisson, Total and effective radiative recombination coefficients, *Astron. Astrophys.* **251**, 680 (1991).
- [55] G. B. Rybicki and A. P. Lightman, *Radiative Processes in Astrophysics* (John Wiley & Sons, Ltd, 1986), [10.1002/9783527618170](https://doi.org/10.1002/9783527618170).
- [56] B. T. Draine, *Physics of the Interstellar and Intergalactic Medium* (Princeton University Press, 2011), [https://books.google.co.jp/books/about/Physics\\_of\\_the\\_Interstellar\\_and\\_Intergal.html?id=FycJvKHyiwsC&redir\\_esc=y](https://books.google.co.jp/books/about/Physics_of_the_Interstellar_and_Intergal.html?id=FycJvKHyiwsC&redir_esc=y).
- [57] S. Weinberg, *Cosmology* (Oxford University Press, New York, 2008).
- [58] G. Nicholson and C. R. Contaldi, Reconstruction of the primordial power spectrum using temperature and polarisation data from multiple experiments, *J. Cosmol. Astropart. Phys.* **07** (2009) 011.
- [59] G. Nicholson, C. R. Contaldi, and P. Paykari, Reconstruction of the primordial power spectrum by direct inversion, *J. Cosmol. Astropart. Phys.* **01** (2010) 016.
- [60] S. Bird, H. V. Peiris, M. Viel, and L. Verde, Minimally parametric power spectrum reconstruction from the Lyman  $\alpha$  forest, *Mon. Not. R. Astron. Soc.* **413**, 1717 (2011).
- [61] E. Komatsu and U. Seljak, The Sunyaev-Zel'dovich angular power spectrum as a probe of cosmological parameters, *Mon. Not. R. Astron. Soc.* **336**, 1256 (2002).